

# ChemComm

Accepted Manuscript



This is an *Accepted Manuscript*, which has been through the Royal Society of Chemistry peer review process and has been accepted for publication.

*Accepted Manuscripts* are published online shortly after acceptance, before technical editing, formatting and proof reading. Using this free service, authors can make their results available to the community, in citable form, before we publish the edited article. We will replace this *Accepted Manuscript* with the edited and formatted *Advance Article* as soon as it is available.

You can find more information about *Accepted Manuscripts* in the [Information for Authors](#).

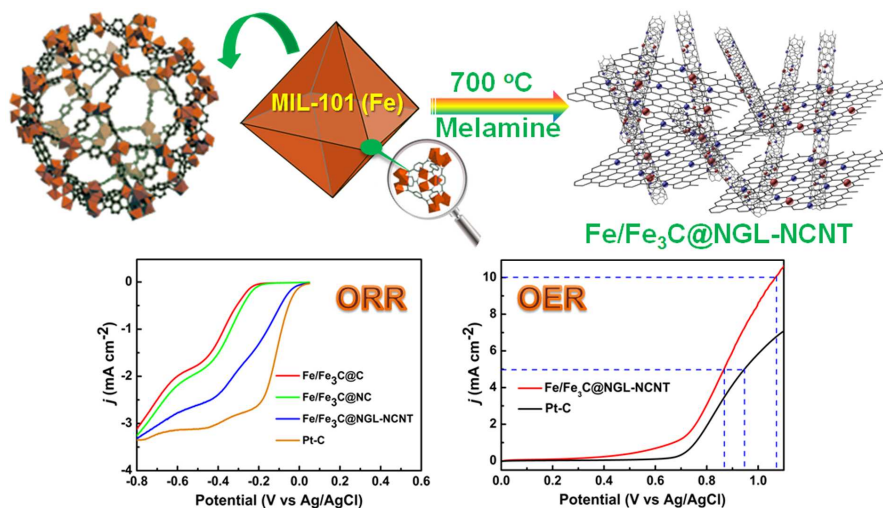
Please note that technical editing may introduce minor changes to the text and/or graphics, which may alter content. The journal's standard [Terms & Conditions](#) and the [Ethical guidelines](#) still apply. In no event shall the Royal Society of Chemistry be held responsible for any errors or omissions in this *Accepted Manuscript* or any consequences arising from the use of any information it contains.

# Graphical abstract

## Nitrogen-doped Fe/Fe<sub>3</sub>C@graphitic layer/carbon nanotube hybrids derived from MOFs: efficient bifunctional electrocatalysts for ORR and OER

Ji-Sen Li,<sup>a,b</sup> Shun-Li Li,<sup>a</sup> Yu-Jia Tang,<sup>a</sup> Min Han,<sup>a</sup> Zhi-Hui Dai,<sup>\*a</sup> Jian-Chun Bao,<sup>a</sup> and Ya-Qian Lan<sup>\*a</sup>

A novel nitrogen-doped Fe/Fe<sub>3</sub>C@graphitic layer/carbon nanotube hybrid derived from MOFs has been first fabricated by a facile approach. The hybrid exhibited outstanding bifunctional electrocatalytic activity for ORR and OER.



## COMMUNICATION

## Nitrogen-doped Fe/Fe<sub>3</sub>C@graphitic layer/carbon nanotube hybrids derived from MOFs: efficient bifunctional electrocatalysts for ORR and OER

Cite this: DOI: 10.1039/x0xx00000x

Received 00th January 2012,  
Accepted 00th January 2012Ji-Sen Li,<sup>a,b</sup> Shun-Li Li,<sup>a</sup> Yu-Jia Tang,<sup>a</sup> Min Han,<sup>a</sup> Zhi-Hui Dai,<sup>\*a</sup> Jian-Chun Bao,<sup>a</sup>  
and Ya-Qian Lan<sup>\*a</sup>

DOI: 10.1039/x0xx00000x

www.rsc.org/

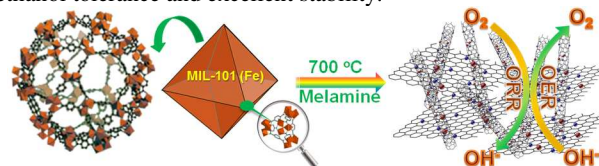
**A novel nitrogen-doped Fe/Fe<sub>3</sub>C@graphitic layer/carbon nanotube hybrid derived from MOFs has been first fabricated by a facile approach. The hybrid exhibited outstanding bifunctional electrocatalytic activity for ORR and OER, due to the merits of graphitic layer/carbon nanotube structures with highly active N and Fe/Fe<sub>3</sub>C sites.**

To solve environmental and energy problems of the world, excellent energy conversion and storage devices, have gained increasing global interest.<sup>1</sup> Electrocatalysts for oxygen reduction (ORR) and evolution reaction (OER) are crucial for practical use such as fuel cells,<sup>2</sup> regenerative metal-air batteries,<sup>3</sup> and water splitting.<sup>4</sup> However, the technical barrier for the development and commercialization of those technologies is the sluggish kinetics of ORR and OER. To date, the state-of-the-art catalysts for ORR are platinum (Pt) and its alloys,<sup>5</sup> and for OER are ruthenium and iridium oxides,<sup>6</sup> respectively. Nevertheless, the high cost as well as limited availability has hampered their widespread and large-scale applications. Accordingly, extensive efforts have been devoted to developing highly efficient, economical, and earth-abundant catalysts for both ORR and OER to replace conventional noble-metal catalysts. Among them, transition metal-nitrogen-carbon (M-N-C) materials,<sup>7</sup> especially for Co-N-C,<sup>8</sup> or Fe-N-C,<sup>9</sup> have been a major focus of research and development, due to their excellent electrocatalytic activity. In particular, it is worth noting that N-doped metal species@carbon hybrids derived from different precursors and synthetic methods have been obtained, which exhibit prominent ORR activity.<sup>10</sup> Nevertheless, most synthetic procedures are extremely complex and involve higher energy consumption, and then greatly limit their practical applications. Despite great efforts, searching for highly efficient and lower cost M-N-C catalyst, especially as an outstanding bifunctional catalyst for ORR and OER, is still of great challenge and significance for the development of renewable energy technologies.

Metal-organic frameworks (MOFs), characteristic of porous crystalline materials, have attracted more attention due to fascinating architectures and excellent properties.<sup>11</sup> Xu's group demonstrated the application of MOFs as precursors for the synthesis of porous carbons for the first time,<sup>12</sup> which can be applied for supercapacitors,<sup>13</sup> gas storage,<sup>14</sup> and so on.<sup>15</sup> Up to now, only a

limited number of electrocatalysts using MOFs as precursors for ORR have been investigated.<sup>16</sup> Most recently, our group has successfully explored heteroatoms dual or ternary-doped porous carbons derived from MOFs as highly efficient metal-free electrocatalysts for ORR.<sup>17</sup> To the best of our knowledge, the N-doped graphitic layer/carbon nanotube hybrids embedded active metal species using MOFs as solid precursors by a facile and in-situ approach remain largely unexplored so far. This material derived from MOFs as solid precursors has two main advantages: (i) in term of porous carbons, hierarchical pores are easily formed using MOFs as precursors; (ii) homogeneous distribution of metal species in MOFs is beneficial for promoting graphitization, further improving its electrocatalytic activity. As a consequence, elaborate design and fabrication of the hybrids derived from MOFs as efficient bifunctional catalysts will be more significant but very challenging.

Herein, this is the first report on the successful synthesis of a novel N-doped Fe/Fe<sub>3</sub>C@graphitic layer/carbon nanotube hybrid (Fe/Fe<sub>3</sub>C@NGL-NCNT) using MOFs as solid precursors by a one-step and in-situ approach. The obtained hybrid, as a bifunctional electrocatalyst, has successfully taken advantage of the merits of Fe species, graphitic layers/carbon nanotubes, and high N content, which shows higher ORR and OER activity, and outstanding methanol tolerance and excellent stability.



**Scheme 1.** Synthesis procedure of Fe/Fe<sub>3</sub>C@NGL-NCNT as a bifunctional electrocatalyst for ORR and OER: blue balls - nitrogen atoms, brown balls - Fe/Fe<sub>3</sub>C species.

MIL-101 (Fe) crystals were synthesized according to the previously reported literature,<sup>18</sup> and the detailed characterizations of MIL-101 (Fe) were shown in Fig. S1 (ESI<sup>†</sup>). The synthetic process for Fe/Fe<sub>3</sub>C@NGL-NCNT was illustrated in Scheme 1 and described in the Experimental Section in detail. For comparison, MIL-101 (Fe), and MIL-101 (Fe) soaked in DMF solution of melamine were also pyrolyzed under the same treatment conditions (denoted as Fe/Fe<sub>3</sub>C@C, and Fe/Fe<sub>3</sub>C@NC), respectively.

The powder X-Ray diffraction (XRD) pattern of the resultant Fe/Fe<sub>3</sub>C@NGL-NCNT is shown in Fig. S2 (ESI<sup>†</sup>). The peak at 26.5° corresponding to the (002) plane of graphitic carbon is observed indicating particular graphitic structures, while the two peaks at around 44.8° and 65.1° are assigned to the (110) and (200) reflections of  $\alpha$ -Fe (JCPDS, No.87-0722), respectively. Apart from the two phases, a certain amount of Fe<sub>3</sub>C (JCPDS, No.89-2867) is also found in the Fe/Fe<sub>3</sub>C@NGL-NCNT sample. These results clarify that the hybrid is composed of Fe/Fe<sub>3</sub>C species and graphitic carbons. Whereas, compared to Fe/Fe<sub>3</sub>C@NGL-NCNT, no graphitic carbon peaks are visible in the XRD patterns of Fe/Fe<sub>3</sub>C@C and Fe/Fe<sub>3</sub>C@NC because the peak intensities are lower than those of Fe/Fe<sub>3</sub>C species. At the same time, this suggests the graphitic degrees of the two samples are lower than that of Fe/Fe<sub>3</sub>C@NGL-NCNT.

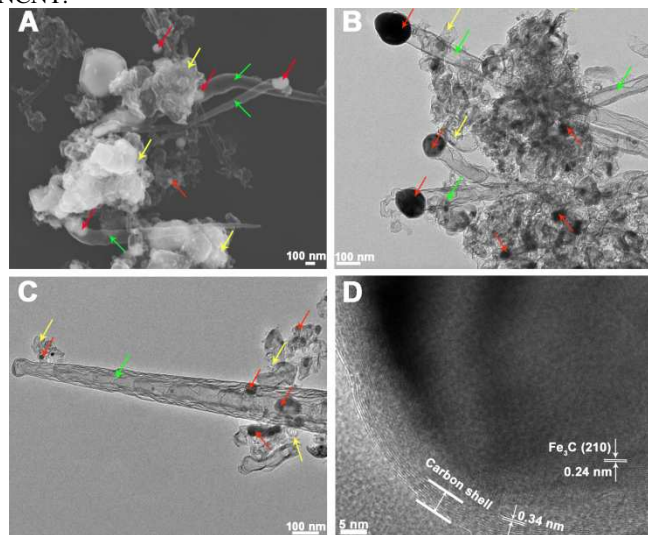


**Fig. 1.** (A) SEM, (B, C) TEM with graphitic layer (yellow arrows), carbon nanotubes (green arrows), and Fe/Fe<sub>3</sub>C (red arrows), and (D) HRTEM image of Fe/Fe<sub>3</sub>C@NGL-NCNT, respectively.

As can be seen from Fig. 1A, scanning electron microscope (SEM) images show the morphologies of graphitic layer (yellow arrows), carbon nanotubes (green arrows), and the embedded Fe/Fe<sub>3</sub>C species (red arrows) as bright dots, which are reconfirmed in the transmission electron microscopy (TEM) images (Fig. 1B). Fig. 1C displays the images of carbon nanotubes with a diameter of about 100 nm. The bamboo-like structures, characteristic of N-doped carbon nanotubes,<sup>10d</sup> are obviously visible. The high-resolution TEM (HRTEM) image in Fig. 1D reveals Fe/Fe<sub>3</sub>C nanoparticles are wrapped in a 5 nm thick graphitic carbon layers with the spacing of 0.34 nm, ascribed to the (002) diffraction plane of graphite.<sup>8a,10d</sup> The dark core distinctly shows a fringe spacing of 0.24 nm corresponding to the (210) plane of Fe<sub>3</sub>C.<sup>10b</sup> Additionally, partial Fe/Fe<sub>3</sub>C nanoparticles are also encapsulated within the graphitic carbon layers,<sup>10c</sup> which is supported by the corresponding elemental mapping (Fig. S3, ESI<sup>†</sup>). This demonstrates that Fe/Fe<sub>3</sub>C species first are embedded into graphitic carbon layers, and then, facilitate the growth of carbon nanotubes.<sup>10d,16d,19</sup> Meanwhile, the graphitic carbon layers efficiently hamper Fe/Fe<sub>3</sub>C species aggregation.

For comparison, the SEM and TEM images of Fe/Fe<sub>3</sub>C@C and Fe/Fe<sub>3</sub>C@NC are also illustrated in Fig. S4 (ESI<sup>†</sup>). Unfortunately, without adding or with a trace amount of melamine, no graphitic layer/carbon nanotubes are presented and Fe/Fe<sub>3</sub>C species are randomly distributed in the porous carbon matrix, consistent with the above XRD patterns. Thus, it confirms that the co-existence of MIL-101 (Fe) and melamine is indispensable for forming the

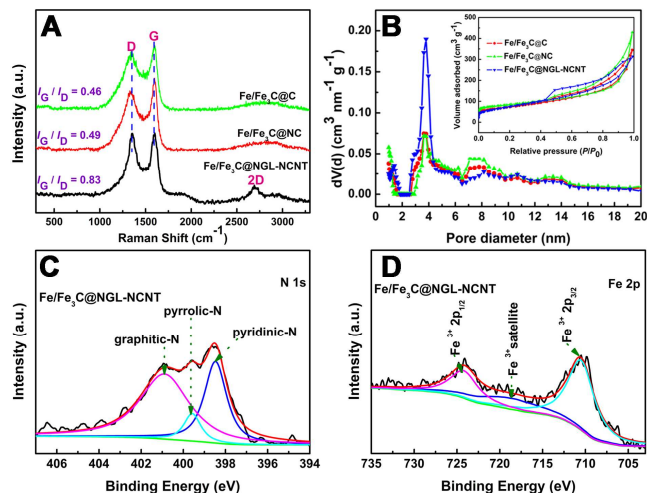


**Fig. 2.** (A) Raman spectra and (B) DFT pore-size distribution curves of different samples. Inset: the N<sub>2</sub> sorption isotherms recorded for different samples. (C, D) High-resolution N 1s and Fe 2p XPS spectra of Fe/Fe<sub>3</sub>C@NGL-NCNT, respectively.

Fe/Fe<sub>3</sub>C@NGL-NCNT composite upon pyrolysis.

The Raman spectrum of Fe/Fe<sub>3</sub>C@NGL-NCNT displays the characteristic G-band at 1590 cm<sup>-1</sup>, and D-band at 1350 cm<sup>-1</sup> (Fig. 2A). In addition, two small peaks are visible at 2700 and 2950 cm<sup>-1</sup>, corresponding to 2D and D + D' bands of graphite,<sup>8a,20</sup> revealing that the graphite component in the Fe/Fe<sub>3</sub>C@NGL-NCNT is a few layers, not a single layer. Additionally, it is found that the I<sub>G</sub>/I<sub>D</sub> of Fe/Fe<sub>3</sub>C@NGL-NCNT is 0.83, higher than that of Fe/Fe<sub>3</sub>C@C (0.46), and Fe/Fe<sub>3</sub>C@NC (0.49), which matches well with the XRD and TEM results. These evidence the higher graphitic degree of Fe/Fe<sub>3</sub>C@NGL-NCNT, which enhances electric conductivity and thus promotes charge transfer.

The N<sub>2</sub> sorption isotherms of different samples are of type IV with distinct hysteresis loops, characteristic of a micro/meso-porous structure (inset of Fig. 2B).<sup>8b,19</sup> The pore size distributions of Fe/Fe<sub>3</sub>C@NGL-NCNT, Fe/Fe<sub>3</sub>C@NC, and Fe/Fe<sub>3</sub>C@C are mainly centered at about 1.2 nm, and 3.8 nm on the basis of the density functional theory (DFT), suggesting that the co-existence of micro/meso-pores in these samples (Fig. 2B). These hierarchical pores are favorable to the adsorption and transportation of O<sub>2</sub>, boosting the ORR activity.

Compared to Fe/Fe<sub>3</sub>C@C (Fig. S5A, ESI<sup>†</sup>), besides C, Fe, and O components, the X-ray photon spectroscopy (XPS) spectra of Fe/Fe<sub>3</sub>C@NC and Fe/Fe<sub>3</sub>C@NGL-NCNT reveal that the presence of N 1s (Fig. S5C-D, ESI<sup>†</sup>). The high resolution XPS N 1s spectrum can be fitted into three peaks, corresponding to graphitic N (~401.2 eV), pyrrolic N (~399.8 eV) and pyridinic N (~398.6 eV) (Fig. 2C, S5E),<sup>2,8c,10d</sup> respectively. Among them, graphitic and pyridinic N are more active than their pyrrolic counterpart, which are advantageous to ORR.<sup>19</sup> In term of Fe 2p spectrum (Fig. 2D, S5B, S5F, ESI<sup>†</sup>), the peaks at 711, 719, and 724 eV are assigned to Fe 2p<sub>3/2</sub>, shake-up satellite Fe 2p<sub>3/2</sub> and Fe 2p<sub>1/2</sub> of Fe<sup>3+</sup>,<sup>21</sup> respectively. Nevertheless, the signal of Fe<sup>0</sup> at 707 eV is not observed, implying that most Fe species are surrounded by carbon layers in the corresponding catalysts. The elemental compositions of different samples are listed in Table S1, in agreement with the energy-dispersive X-ray spectroscopy (EDS) spectra (Fig. S6, ESI<sup>†</sup>). To the best of our knowledge, this is the first report of Fe/Fe<sub>3</sub>C@NGL-NCNT hybrid by a one-step and in-situ approach using MOFs as solid precursors.

The ORR activity of Fe/Fe<sub>3</sub>C@NGL-NCNT in 0.1 M KOH solution was examined by cyclic voltammetry (CV). Compared with no observed current in the N<sub>2</sub>-saturated solution, the O<sub>2</sub> reduction peaks emerge in the O<sub>2</sub>-saturated solution (Fig. S7, ESI<sup>†</sup>). To further

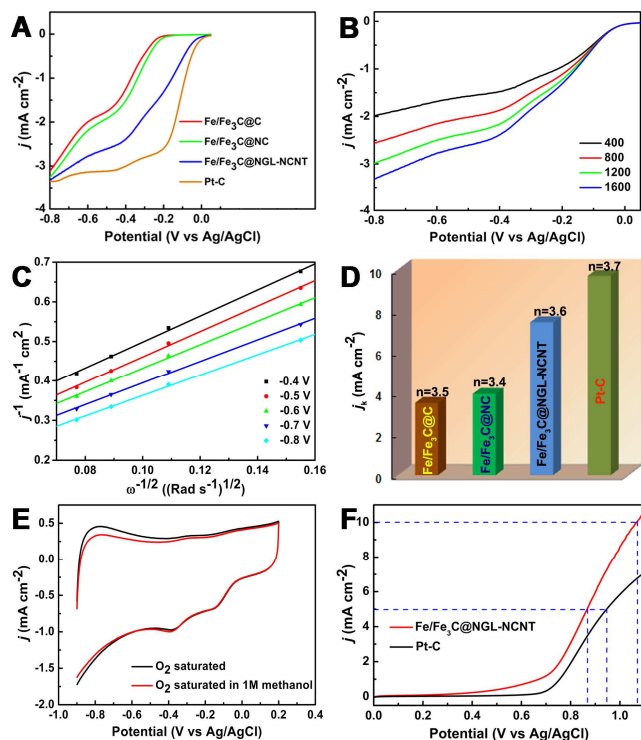


**Fig. 3.** (A) LSVs of different samples at 1600 rpm; (B) LSVs and (C) corresponding K-L plots of Fe/Fe<sub>3</sub>C@NGL-NCNT at various speeds. (D) Kinetic limiting current densities and corresponding electron-transfer numbers of different samples at -0.6 V. (E) CVs of Fe/Fe<sub>3</sub>C@NGL-NCNT in an O<sub>2</sub>-saturated 0.1 M KOH solution or an O<sub>2</sub>-saturated 0.1 M KOH solution upon addition of methanol, respectively. (F) Oxygen evolution currents of the Fe/Fe<sub>3</sub>C@NGL-NCNT, and Pt-C in an O<sub>2</sub>-saturated 0.1 M KOH solution with a sweep rate of 10 mV s<sup>-1</sup>, respectively.

investigate the ORR performance of the composite, linear sweep voltammograms (LSVs) were evaluated by using a rotating-disk electrode (RDE) at a scan rate of 10 mV s<sup>-1</sup> and 1600 rpm. For comparison, other samples and commercial Pt-C were also evaluated under identical conditions, respectively. As seen from Fig. 3A, Fe/Fe<sub>3</sub>C@NGL-NCNT exhibits a higher onset potential (0.04 V) than that of Fe/Fe<sub>3</sub>C@NC (-0.19 V), and Fe/Fe<sub>3</sub>C@C (-0.2 V), very close to commercial Pt-C catalyst (0.045 V) and other reported Pt-free catalysts in an alkaline electrolyte.<sup>10a,21,22</sup> Furthermore, this sufficiently proves that both N and Fe species are crucial for higher electrocatalytic activity, which is in accordance with those of XRD, SEM, TEM, and Raman spectra results.

For the purpose of elucidating the role of Fe/Fe<sub>3</sub>C in the ORR in detail, Fe/Fe<sub>3</sub>C@NGL-NCNT was etched with 2 M H<sub>2</sub>SO<sub>4</sub> at 80 °C for 24 h. From the corresponding SEM, TEM, XRD, N<sub>2</sub> sorption, and LSVs results (Fig. S8-11, ESI<sup>†</sup>), it can be concluded that the Fe/Fe<sub>3</sub>C species make an important contribution to improving the ORR activity.

To further understand the ORR process on these materials, LSVs were then recorded from 400 to 1600 rpm (Fig. 3B) and comparative experiments were provided in Fig. S12A, C (ESI<sup>†</sup>). As the rotation rate increases, the increasing current density is distinctly observed. The relevant Koutecky-Levich (K-L) plots display good linearity from -0.4 V to -0.8 V (Fig. 3C, S12B, D, ESI<sup>†</sup>), implying first-order reaction kinetics for the ORR. Based on the K-L plots, the corresponding electron transfer number (*n*) of Fe/Fe<sub>3</sub>C@NGL-NCNT is estimated to be 3.6, which is higher than that of Fe/Fe<sub>3</sub>C@NC (3.4), and Fe/Fe<sub>3</sub>C@C (3.5), even comparable to Pt-C (3.7) at -0.6 V (Fig. 3D). As well, the corresponding current density of Fe/Fe<sub>3</sub>C@NGL-NCNT is greater than that of the other samples, slight lower than that of commercial Pt-C. Thus, the aforementioned

results clearly highlight that Fe/Fe<sub>3</sub>C@NGL-NCNT has outstanding electrocatalytic activity for ORR in an alkaline electrolyte.

To date, the tolerance to the methanol crossover at cathode reactions plays a pivotal role for the commercialization of fuel cells. From Fig. 3E, when methanol was added, no noticeable change was observed in the CV curves for Fe/Fe<sub>3</sub>C@NGL-NCNT electrode, further demonstrating prominent tolerance to methanol crossover. On the contrary, for commercial Pt-C electrode, the ORR peak disappeared under identical conditions, emerged a new peak ascribed to methanol oxidation reaction (Fig. S13, ESI<sup>†</sup>). This underscores that the Fe/Fe<sub>3</sub>C@NGL-NCNT catalyst is a forceful contender for direct-methanol fuel cells.

OER, as the reverse process of ORR, has attracted more attention in recent years.<sup>4,8c</sup> To further investigate the OER activity of Fe/Fe<sub>3</sub>C@NGL-NCNT, LSV was performed in an O<sub>2</sub>-saturated 0.1 M KOH. In general, the potentials at current densities of 5 mA cm<sup>-2</sup>, and 10 mA cm<sup>-2</sup> are key parameters for OER.<sup>4</sup> From Fig. 3F, the corresponding potential of Fe/Fe<sub>3</sub>C@NGL-NCNT is much lower than that of commercial Pt-C. And then, it further proves that Fe/Fe<sub>3</sub>C@NGL-NCNT is an efficient electrocatalyst for the OER.

For the application of the electrocatalyst, the stability is also an important factor. Fig. S14 (ESI<sup>†</sup>) shows the current-time (*i-t*) chronoamperometric response of Fe/Fe<sub>3</sub>C@NGL-NCNT and Pt-C electrodes at -0.4 V and 0.7 V (vs Ag/AgCl) in O<sub>2</sub>-saturated 0.1 M KOH at a rotation rate of 1600 rpm for the ORR and OER, respectively. Compared to commercial Pt-C catalyst, Fe/Fe<sub>3</sub>C@NGL-NCNT exhibits excellent stability. Therefore, these results further demonstrate that Fe/Fe<sub>3</sub>C@NGL-NCNT is an efficient bifunctional electrocatalyst for energy systems.

Considering the aforementioned results, the prominent electrocatalytic activity of Fe/Fe<sub>3</sub>C@NGL-NCNT is probably attributed to the following reasons: 1) due to the dopant of N, the electroneutrality is broken to explore more active sites, further facilitate the adsorption of O<sub>2</sub> and enhance the ORR activity.<sup>7</sup> 2) The incorporation of the one-dimensional NCNT and two-dimensional NGL is favorable to form the three dimension interpenetrated network structure, further decreasing the internal resistance, and promoting the electron transport.<sup>2,19,23</sup> 3) Fe/Fe<sub>3</sub>C, as active species, are helpful for the formation of CNTs. Additionally, the geometric confinement of Fe/Fe<sub>3</sub>C nanoparticles inside CNTs can significantly improve the catalytic activity for ORR.<sup>8d,21</sup>

In control experiments, the influence of pyrolysis temperature on the ORR was examined in detail (Fig. S15-18, ESI<sup>†</sup>). As shown in Fig. S19 (ESI<sup>†</sup>), Fe/Fe<sub>3</sub>C@NGL-NCNT obtained at 700 °C exhibits the best electrocatalytic activity for the ORR regardless of the onset potential and current density. Accordingly, 700 °C was chosen as the optimal temperature.

In summary, a highly efficient Fe/Fe<sub>3</sub>C@NGL-NCNT hybrid derived from MIL-101 (Fe) has been successfully developed by a facile and in-situ approach for the first time. The influence of pyrolysis temperature on the ORR activity has been investigated in detail. The hybrid, as an efficient bifunctional electrocatalyst, shows higher ORR activity comparable to commercial Pt-C; while methanol tolerance, OER activity and stability superior to those of commercial Pt-C. The excellent activity may originate from the synergistic effect of the unique architecture, large amount of active sites, high N concentration. Consequently, this work paves a new avenue for the design and fabrication of metal species@graphitic layer/carbon nanotube hybrid as an excellent bifunctional electrocatalysts in renewable energy technologies. Appropriate choices of other MOFs, covalent-organic frameworks (COFs), metalloporphyrin-based conjugated porous polymers and so on, should lead to the discovery of a large variety of novel high-efficient multifunctional catalysts in the near future.

This work was financially supported by the NSFC (No. 21175069, 21371099, 21471080, and 21475062), the program of Jiangsu Specially-Appointed Professor, the NSF of Jiangsu Province of China (No. BK20130043), the Natural Science Research of Jiangsu Higher Education Institutions of China (No. 13KJB150021), the Natural Science Foundation of Shandong Province (No. ZR2014BQ037), and the Youths Science Foundation of Jining University (No. 2014QNKJ08).

## Notes and references

<sup>a</sup> Jiangsu Key Laboratory of Biofunctional Materials, College of Chemistry and Materials Science, Nanjing Normal University, Nanjing 210023, P. R. China. E-mail: yqlan@njnu.edu.cn; daizhihui@njnu.edu.cn.

<sup>b</sup> Key Laboratory of Inorganic Chemistry in Universities of Shandong, Department of Chemistry and Chemical Engineering, Jining University, Qufu, 273155, Shandong, P. R. China.

†Electronic Supplementary Information (ESI) available: Full experimental details, Figures and Tables. See DOI: 10.1039/c000000x/

- S. Yang, R. E. Bachman, X. Feng and K. Müllen, *Acc. Chem. Res.*, 2012, **46**, 116.
- P. Chen, T.-Y. Xiao, Y.-H. Qian, S.-S. Li and S.-H. Yu, *Adv. Mater.*, 2013, **25**, 3192.
- (a) Y. Li, M. Gong, Y. Liang, J. Feng, J.-E. Kim, H. Wang, G. Hong, B. Zhang and H. Dai, *Nat. Commun.*, 2013, **4**, 1805; (b) Q. Xiao, Y. Zhang, X. Guo, L. Jing, Z. Yang, Y. Xue, Y.-M. Yan and K. Sun, *Chem. Commun.*, 2014, **50**, 13019; (c) L. Li and A. Manthiram, *J. Mater. Chem. A*, 2013, **1**, 5121; (d) L. Li, S.-H. Chai, S. Dai and A. Manthiram, *Energy Environ. Sci.*, 2014, **7**, 2630.
- Y. Zhao, R. Nakamura, K. Kamiya, S. Nakanishi and K. Hashimoto, *Nat. Commun.*, 2013, **4**, 2390.
- Y. Bing, H. Liu, L. Zhang, D. Ghosh and J. Zhang, *Chem. Soc. Rev.*, 2010, **39**, 2184.
- J. Xu, D. Aili, Q. Li, E. Christensen, J. O. Jensen, W. Zhang, M. K. Hansen, G. Liu, X. Wang and N. J. Bjerrum, *Energy Environ. Sci.*, 2014, **7**, 820.
- F. Jaouen, E. Proietti, M. Lefèvre, R. Chenitz, J.-P. Dodelet, G. Wu, H. T. Chung, C. M. Johnston and P. Zelenay, *Energy Environ. Sci.*, 2011, **4**, 114.
- (a) Z. Xiang, Y. Xue, D. Cao, L. Huang, J.-F. Chen and L. Dai, *Angew. Chem. Int. Ed.*, 2014, **53**, 2433; (b) H.-W. Liang, W. Wei, Z.-S. Wu, X. Feng and K. Müllen, *J. Am. Chem. Soc.*, 2013, **135**, 16002; (c) S. Mao, Z. Wen, T. Huang, Y. Hou and J. Chen, *Energy Environ. Sci.*, 2014, **7**, 609; (d) Z.-S. Wu, L. Chen, J. Liu, K. Parvez, H. Liang, J. Shu, H. Sachdev, R. Graf, X. Feng and K. Müllen, *Adv. Mater.*, 2014, **26**, 1450.
- G. Wu, K. L. More, C. M. Johnston and P. Zelenay, *Science* 2011, **332**, 443.
- (a) J. Liang, R. F. Zhou, X. M. Chen, Y. H. Tang and S. Z. Qiao, *Adv. Mater.*, 2014, **26**, 6074; (b) Z. Wen, S. Ci, F. Zhang, X. Feng, S. Cui, S. Mao, S. Luo, Z. He and J. Chen, *Adv. Mater.*, 2012, **24**, 1399; (c) Y. Hu, J. O. Jensen, W. Zhang, L. N. Cleemann, W. Xing, N. J. Bjerrum and Q. Li, *Angew. Chem. Int. Ed.*, 2014, **53**, 3675; (d) H. T. Chung, J. H. Won and P. Zelenay, *Nat. Commun.*, 2013, **4**, 1922.
- S.-L. Li and Q. Xu, *Energy Environ. Sci.*, 2013, **6**, 1656.
- B. Liu, H. Shioyama, T. Akita and Q. Xu, *J. Am. Chem. Soc.*, 2008, **130**, 5390.
- W. Chaikittisilp, M. Hu, H. Wang, H.-S. Huang, T. Fujita, K. C. W. Wu, L.-C. Chen, Y. Yamauchi and K. Ariga, *Chem. Commun.*, 2012, **48**, 7259.
- S. J. Yang, T. Kim, J. H. Im, Y. S. Kim, K. Lee, H. Jung and C. R. Park, *Chem. Mater.*, 2012, **24**, 464.
- N. L. Torad, M. Hu, S. Ishihara, H. Sukegawa, A. A. Belik, M. Imura, K. Ariga, Y. Sakka and Y. Yamauchi, *Small* 2014, **10**, 2096.
- (a) E. Proietti, F. Jaouen, M. Lefevre, N. Larouche, J. Tian, J. Herranz and J. P. Dodelet, *Nat. Commun.*, 2011, **2**, 416; (b) S. Ma, G. A. Goenaga, A. V. Call and D.-J. Liu, *Chem. Eur. J.*, 2011, **17**, 2063; (c) D. Zhao, J.-L. Shui, C. Chen, X. Chen, B. M. Reprogle, D. Wang and D.-J. Liu, *Chem. Sci.*, 2012, **3**, 3200; (d) P. Su, H. Xiao, J. Zhao, Y. Yao, Z. Shao, C. Li and Q. Yang, *Chem. Sci.*, 2013, **4**, 2941; (e) J. Tian, A. Morozan, M. T. Sougrati, M. Lefèvre, R. Chenitz, J.-P. Dodelet, D. Jones and F. Jaouen, *Angew. Chem. Int. Ed.*, 2013, **52**, 6867; (f) D. Zhao, J.-L. Shui, L. R. Grabstanowicz, C. Chen, S. M. Commet, T. Xu, J. Lu and D.-J. Liu, *Adv. Mater.*, 2014, **26**, 1093; (g) S. Pandiaraj, H. B. Aiyappa, R. Banerjee and S. Kurungot, *Chem. Commun.*, 2014, **50**, 3363.
- (a) J. Li, Y. Chen, Y. Tang, S. Li, H. Dong, K. Li, M. Han, Y.-Q. Lan, J. Bao and Z. Dai, *J. Mater. Chem. A*, 2014, **2**, 6316; (b) J.-S. Li, S.-L. Li, Y.-J. Tang, K. Li, L. Zhou, N. Kong, Y.-Q. Lan, J.-C. Bao and Z.-H. Dai, *Sci. Rep.*, 2014, **4**, 5130.
- N. V. Maksimchuk, K. A. Kovalenko, V. P. Fedin and O. A. Kholdeeva, *Chem. Commun.*, 2012, **48**, 6812.
- Q. Li, P. Xu, W. Gao, S. Ma, G. Zhang, R. Cao, J. Cho, H.-L. Wang and G. Wu, *Adv. Mater.*, 2014, **26**, 1378.
- G. Wu, N. H. Mack, W. Gao, S. Ma, R. Zhong, J. Han, J. K. Baldwin and P. Zelenay, *ACS Nano*, 2012, **6**, 9764.
- D. Deng, L. Yu, X. Chen, G. Wang, L. Jin, X. Pan, J. Deng, G. Sun and X. Bao, *Angew. Chem. Int. Ed.*, 2013, **52**, 371.
- (a) Z. S. Wu, S. Yang, Y. Sun, K. Parvez, X. Feng and K. Müllen, *J. Am. Chem. Soc.*, 2012, **134**, 9082; (b) C. Zhang, N. Mahmood, H. Yin, F. Liu and Y. Hou, *Adv. Mater.*, 2013, **25**, 4932; (c) Y. Zheng, Y. Jiao, L. Ge, M. Jaroniec and S. Z. Qiao, *Angew. Chem. Int. Ed.*, 2013, **52**, 3110.
- (a) Z. Fan, J. Yan, L. Zhi, Q. Zhang, T. Wei, J. Feng, M. Zhang, W. Qian and F. Wei, *Adv. Mater.*, 2010, **22**, 3723. (b) R. Lv, E. Cruz-Silva and M. Terrones, *ACS Nano*, 2014, **8**, 4061.